Monthly Notices
of the
ROYAL ASTRONOMICAL SOCIETY

Mon. Not. R. Astron. Soc. **424,** 1522–1529 (2012) doi:10.1111/j.1365-2966.2012.21344.x

Predictions for the intrinsic UV continuum properties of star-forming galaxies and the implications for inferring dust extinction

Stephen M. Wilkins,[1⋆] Violeta Gonzalez-Perez,[2] Cedric G. Lacey[2] and Carlton M. Baugh[2]

[1] *University of Oxford, Department of Physics, Denys Wilkinson Building, Keble Road, Oxford OX1 3RH*
[2] *Institute for Computational Cosmology, Department of Physics, University of Durham, South Road, Durham DH1 3LE*

Accepted 2012 May 18. Received 2012 May 15; in original form 2012 March 30

ABSTRACT

The observed ultraviolet continuum (UVC) slope is potentially a powerful diagnostic of dust obscuration in star-forming galaxies. However, the intrinsic slope is also sensitive to the form of the stellar initial mass function and to the recent star formation and metal enrichment histories of a galaxy. Using the GALFORM semi-analytical model of galaxy formation, we investigate the intrinsic distribution of UVC slopes. For star-forming galaxies, we find that the intrinsic distribution of UVC slopes at $z = 0$, parametrized by the power-law index β, has a standard deviation of $\sigma_\beta \simeq 0.30$. This suggests an uncertainty on the inferred ultraviolet (UV) attenuation of $A_{\rm fuv} \simeq 0.7$ (assuming a Calzetti attenuation curve) for an individual object, even with perfect photometry. Furthermore, we find that the intrinsic UVC slope correlates with star formation rate, intrinsic UV luminosity, stellar mass and redshift. These correlations have implications for the interpretation of trends in the observed UVC slope with these quantities irrespective of the sample size or quality of the photometry. Our results suggest that in some cases the attenuation by dust has been incorrectly estimated.

Key words: galaxies: formation – ultraviolet: galaxies.

1 INTRODUCTION

The ultraviolet continuum (UVC) slope has been proposed as a robust diagnostic of dust attenuation in star-forming galaxies (e.g. Meurer, Heckman & Calzetti 1999). The usefulness of the UVC slope is most apparent at high redshift where alternative diagnostics of dust attenuation such as the far-infrared are generally inaccessible and galaxies are selected on the basis of their rest-frame ultraviolet (UV) emission (e.g. Wilkins et al. 2010, 2011a). This has prompted several studies which carefully study the UVC slopes of high-redshift galaxies in an attempt to constrain the degree of dust obscuration in UV selected samples (e.g. Bouwens et al. 2009, 2011; Wilkins et al. 2011b; Dunlop et al. 2012; Finkelstein et al. 2012).

In all of these studies, a simple linear relation is assumed between the observed UVC slope and the amount of dust attenuation. This requires the assumption of a unique *intrinsic* UVC slope. However, the intrinsic UVC slope is also affected by a number of other properties besides dust, including the recent star formation (SF) and metal enrichment histories, and the form of the stellar initial mass function (IMF). The sensitivity of the intrinsic slope to these properties potentially limits the usefulness of the observed UVC slope as an accurate diagnostic of dust attenuation. In this work, we employ the GALFORM semi-analytical model of galaxy formation (first developed by Cole et al. 2000) to produce realistic SF and metal enrichment histories with which to determine the intrinsic distribution of UVC slopes $\beta_{\rm i}$ and to investigate how this distribution varies with stellar mass, SF rate, UV luminosity and redshift. Lacey et al. (2011) have shown that this model can reproduce the observed UV luminosity function over a wide range of redshifts (see also Gonzalez-Perez et al., in preparation).

This paper is organized as follows. In Sections 2.1 and 2.2, we introduce the GALFORM semi-analytical galaxy formation model and filter convention, respectively. In Section 3, we discuss the principal physical properties which affect the observed UVC and investigate, using the PEGASE.2 stellar population synthesis (SPS) model (Fioc & Rocca-Volmerange 1997, 1999), how the UVC slope is affected by dust and changes in the recent SF and metal enrichment histories, and by the choice of IMF. In Section 3, we also investigate the distribution of UVC colours/slopes predicted by the GALFORM model as a result of the predicted variety in the star formation history (SFH) alone (Section 3.2) and in the metal enrichment history (Section 3.3). In Section 4, we investigate how the distribution of intrinsic UVC slopes is affected by the SF rate (Section 4.1), intrinsic UV luminosity (Section 4.2), stellar mass

⋆E-mail: stephen.wilkins@physics.ox.ac.uk

(Section 4.3) and redshift (Section 4.4). In Section 5, we present our conclusions.

2 MODELLING APPROACH

In this section, we give an overview of the GALFORM galaxy formation model (Section 2.1) and set out how the UVC slope is measured (Section 2.2).

2.1 The galaxy formation model

We predict the intrinsic UVC slope of galaxies in a Λ cold dark matter universe using the GALFORM semi-analytical galaxy formation model developed by Cole et al. (2000). Semi-analytical models use physically motivated equations to follow the fate of baryons in a universe in which structure grows hierarchically through gravitational instability (see Baugh 2006 for an overview of hierarchical galaxy formation models).

GALFORM follows the main processes which shape the formation and evolution of galaxies. These include: (i) the collapse and merging of dark matter haloes; (ii) the shock heating and radiative cooling of gas inside dark matter haloes, leading to the formation of galaxy discs; (iii) quiescent SF in galaxy discs; (iv) feedback from supernovae, from active galactic nuclei and from photoionization of the intergalactic medium (IGM); (v) chemical enrichment of stars and gas and (vi) galaxy mergers driven by dynamical friction within common dark matter haloes, leading to the formation of stellar spheroids, which also may trigger bursts of SF. The end product of the calculation is a prediction for the number and properties of galaxies which reside within dark matter haloes of different masses. The outputs include the SF and metal enrichment histories for each galaxy, including the contribution of merger-driven starbursts. The SFHs predicted by the model are in general more complex than the exponentially decaying models typically assumed to interpret observations (see Baugh 2006 for examples).

In this paper, we focus our attention on the Baugh et al. 2005 (hereafter B05) model. Some of the key features of this model are: (i) a time-scale for quiescent SF that is assumed to vary as a power of the disc circular velocity (see Lagos et al. 2011 for a study of different SF laws in quiescent galaxies); (ii) bursts of SF are triggered only by galaxy mergers; (iii) the *default* implementation of this model adopts a Kennicutt (1983) IMF ($\xi = \mathrm{d}N/\mathrm{d}m \propto m^{-2.5}$ for $m > 1\,\mathrm{M}_\odot$ and $\xi \propto m^{-1.4}$ for $m < 1\,\mathrm{M}_\odot$; cf. Salpeter 1955: $\xi \propto m^{-2.35}$) in quiescent SF in galactic discs, while in starbursts a top-heavy IMF ($\xi \propto m^{-1}$) is assumed; (iv) the inclusion of supernova feedback with superwinds (see Benson et al. 2003 for a discussion of the effect that feedback has on the luminosity function of galaxies) and (v) the reionization of the IGM is approximated by a simple model in which gas cooling is completely suppressed in haloes with circular velocities less than $30\,\mathrm{km\,s^{-1}}$ at redshifts $z < 10$ (Lacey et al. 2011). The parameters of this model were fixed with reference to a subset of the available observations of galaxies, mostly at low redshift. The B05 model uses, by default, the simple stellar population spectral energy distributions (SEDs) generated by Bressan, Granato & Silva (1998), using the Padova 1994 stellar evolution tracks and the model stellar atmospheres from Kurucz (1993).[1] The B05 model uses the canonical (ΛCDM) parameters: matter density, $\Omega_0 = 0.3$, cosmological constant, $\Omega_\Lambda = 0.7$, baryon density, $\Omega_\mathrm{b} = 0.04$, a normalization of density fluctuations given by $\sigma_8 = 0.93$ and a Hubble constant today $H_0 = 70\,\mathrm{km\,s^{-1}\,Mpc^{-1}}$. The B05 model employs merger trees generated using the Monte Carlo algorithm introduced by Parkinson, Cole & Helly (2008). The B05 model also includes a dust model in which stars and dust are mixed together. The dust extinction in GALFORM and the impact on the rest-frame UV are discussed in Lacey et al. (2011) and Gonzalez-Perez et al. (in preparation). In the calculations presented here, we study the intrinsic UVC predicted by GALFORM and so omit dust extinction in the model predictions.

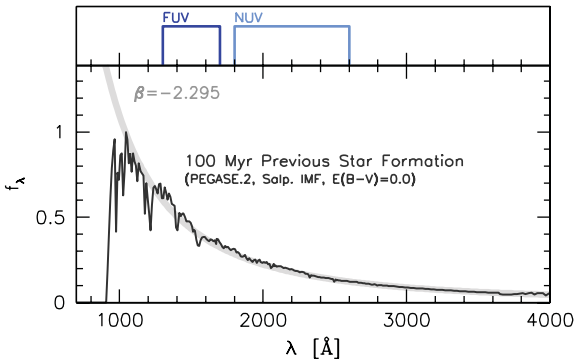

Figure 1. The synthetic UV spectrum of a star-forming galaxy (100 Myr of previous continuous SF, Salpeter IMF, $Z = \mathrm{Z}_\odot$) produced with the PEGASE.2 population synthesis model (black line). The heavy grey line is a pure power law $f_\lambda \propto \lambda^\beta$ assuming the value of β inferred from the FUV−NUV colour (transmission functions shown in the upper panel).

In addition to reproducing local galaxy data, the B05 model matches the number and redshift distribution of galaxies detected by their emission at submillimetre wavelengths, the luminosity function of Lyman-break galaxies and the abundance and clustering of Lyman α emitters (Orsi et al. 2008). No parameters have been tuned for the study presented here. We refer the reader to B05 and Lacey et al. (2008, 2011) for a full description of this model. As a method of exploring differences in the distribution of UVC slopes arises from the IMF, SFH and metal enrichment history, we consider three separate implementations of the B05 model.

(i) Default – the default implementation of the model as described by B05.

(ii) Single IMF – same as the default implementation except that the top-heavy IMF in starbursts is replaced by the Kennicutt IMF, so this IMF is used in all modes of SF.

(iii) Single IMF + single metallicity – same as the default implementation except that the top-heavy IMF in starbursts is replaced by the Kennicutt IMF and all stars are assumed to have the same metallicity ($Z = \mathrm{Z}_\odot$).

2.2 Filters

In order to reproduce the techniques commonly applied to observations, we measure the UVC slope using two artificial broad-band rest-frame filters (shown in Fig. 1): far-ultraviolet (FUV) ($T_\lambda = [0.13 < \lambda/\mu\mathrm{m} < 0.17]$[2]) and near-ultraviolet (NUV) ($T_\lambda = [0.18 < \lambda/\mu\mathrm{m} < 0.26]$). These filters cover a similar wavelength range to the *GALEX* filter set. The use of rest-frame filters

[1] These are the same isochrones and stellar atmospheres as used by Bruzual & Charlot (2003).

[2] We utilize the Iverson bracket notation such that $[A] = 1$ when A is true and 0 otherwise.

allows us to consistently compare the distribution of UVC slopes in galaxies at different redshifts.

2.2.1 Parametrization of the UVC slope

Observations of the UVC colours of galaxies at different redshifts are difficult to compare as in each case the available filters probe different ranges of the UVCs. To compare the UVC properties at different redshifts it is instead common to parametrize the continuum by a power law, with slope β, i.e.

$$f_\lambda \propto \lambda^\beta, \tag{1}$$

or in terms of f_ν,

$$f_\nu \propto \lambda^{2+\beta}. \tag{2}$$

In the context of our choice of rest-frame filters, the conversion from the $(\mathrm{FUV}-\mathrm{NUV})_{\mathrm{AB}}$ colour to β is

$$\beta = C \times (\mathrm{FUV}-\mathrm{NUV})_{\mathrm{AB}} - 2, \tag{3}$$

where C is a conversion factor determined by convolving the two filter transmission functions with a power-law spectrum. The value of C is sensitive to the individual filters[3] and for the FUV and NUV filters defined above it is 2.49. Fig. 1 shows both the synthetic UV spectrum of a star-forming galaxy and the power law using the value of β inferred from the FUV−NUV colour.

Throughout this work, we make a distinction between the *intrinsic* UVC slope β_{i} and the observed slope β_{o}. The intrinsic slope is assumed to be the slope produced by stars in the absence of any extrinsic effects such as dust extinction or nebular emission.

3 PHYSICAL PROPERTIES AFFECTING THE OBSERVED UVC SLOPE

The observed UVC slope of a galaxy is affected by various properties both intrinsic and extrinsic to the stars producing the UV emission.

The intrinsic UVC of actively star-forming galaxies is dominated by emission from the most massive, high-temperature stars ($m > 2\,\mathrm{M}_\odot$, OBA class). The UV ($1216 \rightarrow 3000$ Å) spectral flux density of these stars is well characterized by a power law with a *blue* slope (i.e. if $f_\nu \propto \lambda^{2+\beta}$ then $\beta < -2$) as shown in Fig. 1. This power-law behaviour principally arises because the UVC probes the Rayleigh–Jeans tail of the blackbody SED (though it deviates from a pure Rayleigh–Jeans behaviour because of the effects of opacity in the star's atmosphere) as shown by the synthetic spectrum in Fig. 1. At lower temperatures, the range $1216 \rightarrow 3000$ Å probes where the blackbody distribution peaks. This effect, combined with variation in the opacity (as a function of temperature, etc.), results in the SEDs of the cooler, lower mass stars having a redder UVC than those of stars with higher temperatures/masses. The sensitivity of the UVC of a star to its temperature (and opacity), and thus metallicity, mass and age, means that the intrinsic continuum of a composite stellar population is sensitive to the distribution of stellar masses, ages and metallicities. The distribution of masses is in turn determined by the SFH and IMF; thus both these factors affect the *intrinsic* UVC colours.

In addition to these intrinsic properties, the *observed* UVC is also affected by the presence of intervening dust through scattering and absorption, and (typically to a much lesser extent) continuum emission from hot ionized gas.

In the following sections (Sections 3.1–3.4), we both outline the effect of dust (Section 3.1) and investigate the effect of intrinsic properties (including the SFH, metallicity and IMF) on the observed UVC colours/slope.

3.1 Dust

The principal property which causes the observed UVC slope β_{o} of luminous star-forming galaxies to differ from the intrinsic slope is dust. Both empirically determined (e.g. Cardelli, Clayton & Mathis 1989; Calzetti et al. 2000, hereafter C00[4]) and theoretically motivated dust attenuation laws suggest that attenuation increases rapidly from the NIR/optical through the UV. As such, the UV colour is potentially a powerful diagnostic of dust attenuation as the presence of dust will redden the observed slope compared to its intrinsic value. The exact relation depends on the characteristics of the attenuation curve in the UV; for example, depending on the choice of filters and redshift, a curve including the bump feature at $\lambda = 2175$ Å (such as the Cardelli et al. 1989 extinction curve) implies a much weaker relationship between the UVC slope and dust than the C00 attenuation curve which decreases monotonically with wavelength.

Here we use the C00 attenuation curve to see the effect of dust on the observed UVC slope. Assuming that the underlying intrinsic UVC is described by a power law (equation 2), a relationship between the observed and intrinsic UVC slopes, β_{o} and β_{i}, respectively, and the attenuation in the FUV, A_{fuv}, can be derived (cf. C00),

$$A_{\mathrm{fuv}} = 2.37 \times [\beta_{\mathrm{o}} - \beta_{\mathrm{i}}]. \tag{4}$$

Assuming a synthetic intrinsic UVC (produced in this example using the PEGASE.2 SPS model) corresponding to 100 Myr previous constant SF, and a Salpeter IMF with solar metallicity (as shown in Fig. 1) yields an intrinsic UVC slope of $\beta_{\mathrm{i}} \simeq -2.3$. Inserting this into equation (4) yields

$$A_{\mathrm{fuv}} = 2.37\beta_{\mathrm{o}} + 5.5, \tag{5}$$

which is similar to the relation proposed by Meurer et al. (1999). This can be rewritten to express the uncertainty on the attenuation arising from the uncertainty in the intrinsic UVC slope,

$$\delta A_{\mathrm{fuv}} = 2.37 \times \delta\beta_{\mathrm{i}}. \tag{6}$$

This highlights the strong dependence of the inferred UV attenuation on the intrinsic UVC slope.

3.2 Star formation history

The strong variation with mass of the main-sequence lifetimes of stars means that the contemporary mass distribution, and thus UVC slope, is sensitive to a galaxy's SFH. After less than 10 Myr of continuous SF, a stellar population would still retain most of its original high-mass stars (i.e. up to this time, the contemporary mass distribution is similar to the IMF). However, after prolonged periods of SF, some fraction of the most massive stars will have evolved off the main sequence. This reduces the relative contribution of these stars to the UVC, resulting in a redder slope (i.e. $\beta > -2$).

[3] For a combination of observer frame filters C is also sensitive to the source redshift.

[4] The C00 *starburst* attenuation curve encapsulates the effects of scattering and absorption while the Cardelli et al. (1989) curve describes extinction by a foreground screen and includes the prominent bump at $\lambda = 2175$ Å.

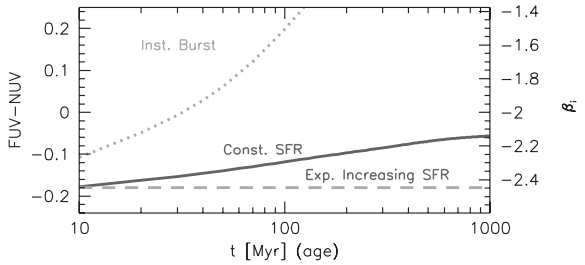

Figure 2. The effect of the duration and form of previous SF on the UVC colour. The three lines show the evolution of the UVC colour (left) and slope (right) of a stellar population-forming stars at a constant rate (solid line), an exponentially increasing rate (dashed line) and as an instantaneous burst (dotted line).

The limiting cases of the effect of the previous SFH are shown in Fig. 2. Here the evolution of the UVC slope is shown for three cases: an instantaneous burst, a constant SFH and an exponentially increasing SFH (assuming solar metallicity and a Salpeter IMF). The last case essentially leaves the slope constant, as the UVC is continuously dominated by the most massive OB-type stars. In the first case, the intrinsic UVC slope quickly reddens as it becomes dominated by progressively cooler stars. For the intermediate case, corresponding to a constant SF rate, the intrinsic UVC slope evolves mildly, changing by only $\delta\beta_i \simeq 0.3$ between SF durations of 10 Myr and 1 Gyr.

Fig. 2 highlights that the UVC slope is sensitive to the recent SFH. Estimating the uncertainty on the intrinsic UVC slope, $\delta\beta_i$, requires knowledge of the range of SFHs. To obtain these, we use simulated galaxies taken from the GALFORM model. In order to investigate the effect of the SFH on the UVC, we consider special cases in which the model is run with a fixed (solar) metallicity and a single IMF (Kennicutt 1983), with the variation in the intrinsic UVC slope then being entirely due the effect of the SFH. The resulting distribution of UVC slopes, for galaxies selected as star forming (i.e. with SF rates $\psi > 0.1\,M_\odot\,yr^{-1}$), is shown in Fig. 3. The structure of this distribution is asymmetric with a long red tail. The asymmetry in the distribution (and the long red tail) is driven by the fact that while

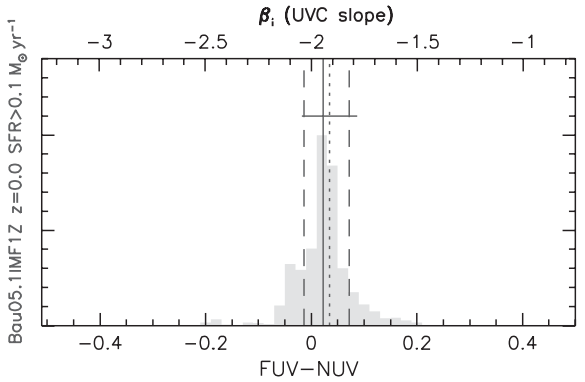

Figure 3. The simulated distribution of intrinsic UVC slopes (top axis) and colours (bottom axis) for star-forming galaxies (defined as those with SFR $> 0.1\,M_\odot\,yr^{-1}$) in the GALFORM model at $z = 0$, assuming a single *constant* metallicity and universal IMF. The solid, dotted and dashed vertical lines denote the weighted mean, median and the 15.87–84.13th percentile range, respectively. The solid horizontal line shows the standard deviation around the median. This, and subsequent, histograms are normalized by the modal value.

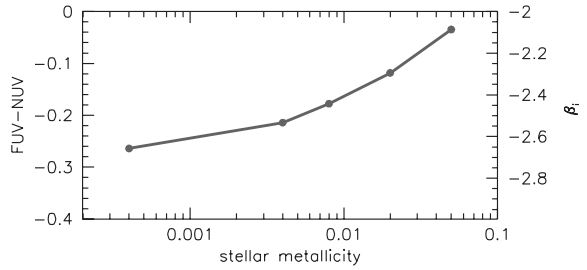

Figure 4. The effect of assuming different values of the stellar metallicity on the intrinsic UVC colour (left) and slope (right) derived from the PEGASE.2 SPS model (assuming a 100 Myr previous duration of continuous SF prior to measurement and a Salpeter IMF).

it is possible to obtain extremely red UVC slopes by having a dominant old stellar population, it is impossible to push the UVC slope to be arbitrarily blue. Despite the non-Gaussian structure of this distribution, the standard deviation around the median provides a close indication of the 15.87–84.13th percentile confidence interval. The standard deviation of this distribution is $\sigma_\beta \simeq 0.13$; assuming the formula relating the uncertainty on β_i to the UV attenuation (equation 6), this suggests an intrinsic uncertainty on the UV attenuation due to the variation in the SFH of the galaxy population of $\delta A_{fuv} \simeq 0.31$.

3.3 Metallicity

Both the opacities and effective temperatures, and thus the UVCs, of stars are affected by their chemical composition; stars with lower metal abundances typically have bluer UVC slopes. Hence, the intrinsic UVC slope is also sensitive to the metallicity of the UV luminous population, or specifically to the *recent* metal enrichment history. Fig. 4 shows the impact of metallicity on the intrinsic UVC slope (assuming constant SF in the 100 Myr prior to observation and a Salpeter (1955) IMF, using the PEGASE.2 population synthesis model); changing the metallicity from $Z = 0.02$ to 0.004 causes the intrinsic UVC slope β_i to steepen by $\simeq$0.25. Thus the UV attenuation, A_{fuv}, of a galaxy which has $Z = 0.004$, but which is assumed to have $Z = 0.02$, would be overestimated by $\simeq$0.6 mag due to the difference in the intrinsic UVC colour.

As with the SFH, accounting for the metallicity effects is difficult without some knowledge of the metal enrichment history. Once again, we turn to the GALFORM model to provide plausible distributions of SF and metal enrichment histories from which we can determine the intrinsic UVC slope. Including the predicted variation in metal enrichment histories of galaxies widens the intrinsic distribution of UVC slopes compared to that obtained assuming a single metallicity (the resulting distribution is shown in Fig. 5). The standard deviation of the intrinsic UVC slope distribution increases to $\sigma_\beta \simeq 0.30$ compared with $\sigma_\beta \simeq 0.13$ with no metallicity variation. Using equation (6), this suggests an intrinsic uncertainty in the UV attenuation inferred from the UVC colour of $\delta A_{fuv} \simeq 0.7$. This suggests that, even in the absence of photometric noise or redshift uncertainties, the dust attenuation of a single object cannot be measured more accurately than $\delta A_{fuv} \simeq 0.7$ without additional information to constrain the SFH or metallicity.

3.4 Initial mass function

The IMF ($\xi(m) = dN/dm$) describes the stellar mass distribution of a single stellar population with $t_{age} = 0$. A range of parametrizations of

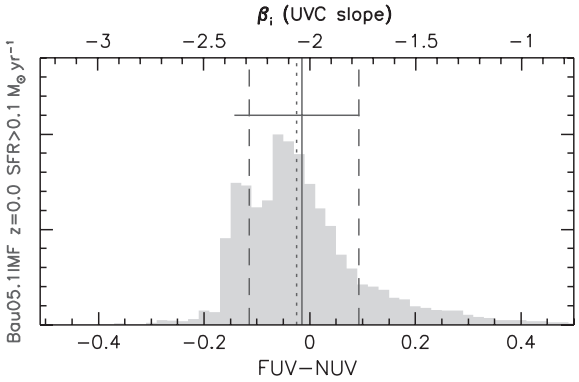

Figure 5. The simulated distribution of UVC colours for star-forming galaxies (SFR $> 0.1\,\mathrm{M}_\odot\,\mathrm{yr}^{-1}$) at $z = 0$ assuming a single IMF but varying metal enrichment and SFH. The solid, dotted and dashed vertical lines denote the weighted mean, median and 15.87–84.13th percentile range, respectively. The solid horizontal line shows the standard deviation around the median.

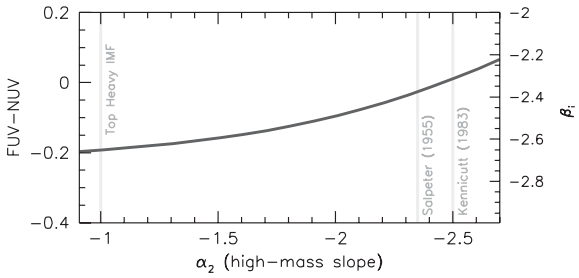

Figure 6. The effect of the choice of the high-mass slope α_2 of the IMF on the UVC colour/slope derived from the PEGASE.2 SPS mode (assuming a 100 Myr previous duration of continuous SF and solar metallicity).

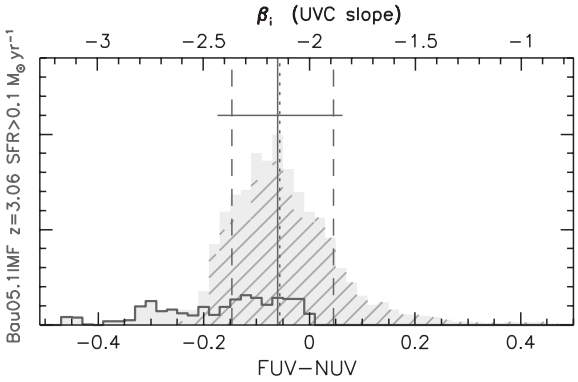

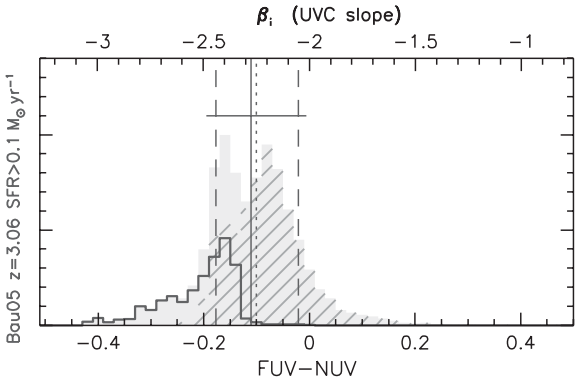

Figure 7. The simulated distribution of intrinsic UVC colours and slopes for star-forming galaxies ($\psi > 0.1\,\mathrm{M}_\odot\,\mathrm{yr}^{-1}$) at $z = 3$ assuming the B05 model with a single Kennicutt (1983) IMF (top) and the default implementation with two IMFs (bottom). The histogram enclosed by the dark line shows the distribution for galaxies whose total SF is dominated by the burst mode while the hatched histogram shows those dominated by quiescent SF (the grey shaded histogram is for all star-forming galaxies).

the IMF exist, with the simplest one taking the form of a single power law (i.e. $\xi(m) \propto m^\alpha$), e.g. the Salpeter (1955) IMF with $\alpha = -2.35$. Updated parametrizations take into account the observed flattening of the IMF below some characteristic mass (e.g. $m_\mathrm{c} \simeq 1\,\mathrm{M}_\odot$ for the Kennicutt IMF) by adopting a broken power law parametrized by α_1 and α_2 (the low- and high-mass slopes respectively).

The IMF can be modified in a number of ways in the context of this parametrization. One method is to simply vary the high-mass slope α_2. Steepening the high-mass slope (decreasing α_2) will reduce the relative contribution of very high mass stars to the UV luminosity; this will have the effect of reddening the UVC colour/slope. This can be seen in Fig. 6 (assuming 100 Myr previous duration of continuous SF and solar metallicity); flattening α_2 from -2.35 to -1.5 reduces the slope by $\Delta\beta_\mathrm{i} \simeq 0.2$ assuming the same SF and metal enrichment history.

The effect of the IMF is potentially important as a number of studies have suggested that the high-mass slope of the IMF may be flatter than Salpeter (e.g. Wilkins, Trentham & Hopkins 2008b) or that the IMF may *effectively* vary from galaxy to galaxy (e.g. Baldry & Glazebrook 2003; Hoversten & Glazebrook 2008; Wilkins et al. 2008a; Lee et al. 2009; Finkelstein et al. 2011).

The *default* implementation of the B05 GALFORM model adopts a top-heavy IMF ($\xi \propto m^{-1}$) in merger-triggered SF, while retaining the Kennicutt IMF in quiescent SF. At low redshift, where our attention has been focused thus far, the fraction of SF occurring with the flat, top-heavy IMF is small in the B05 model. This fraction increases with redshift such that at $z \simeq 3$ the contribution to the SF rate density from each mode is roughly similar. In Fig. 7, we compare the intrinsic UVC slope distribution of galaxies at $z \simeq 3$ using both the default implementation of the B05 model (i.e. with the top-heavy IMF mode of SF in bursts) and a variant in which a universal IMF is used. The main difference between the two is that the distribution of UVC colours in the default B05 model is on average bluer and the width of the distribution slightly smaller. A second peak also emerges associated with burst-driven SF. This can be seen clearly in Fig. 7 where the distribution for galaxies whose total SF is dominated by the burst mode is shown alongside the full distribution.

4 TRENDS WITH SFR, UV LUMINOSITY, STELLAR MASS AND REDSHIFT

In the previous section, we showed that the distribution of intrinsic UVC slopes (of star-forming galaxies) is affected by the IMF, and the SF and metal enrichment histories of galaxies. In this section, we investigate if the median intrinsic UVC slope correlates with a galaxy's SF rate, intrinsic UV luminosity, stellar mass and redshift. A correlation of the intrinsic slope with any of these properties may result in an erroneous observed correlation between the property and the inferred dust extinction, or may reinforce a weak or negligible correlation.

Fig. 8 shows the median intrinsic UVC slope for the three variants of the B05 model (single-IMF and single-metallicity, single-IMF

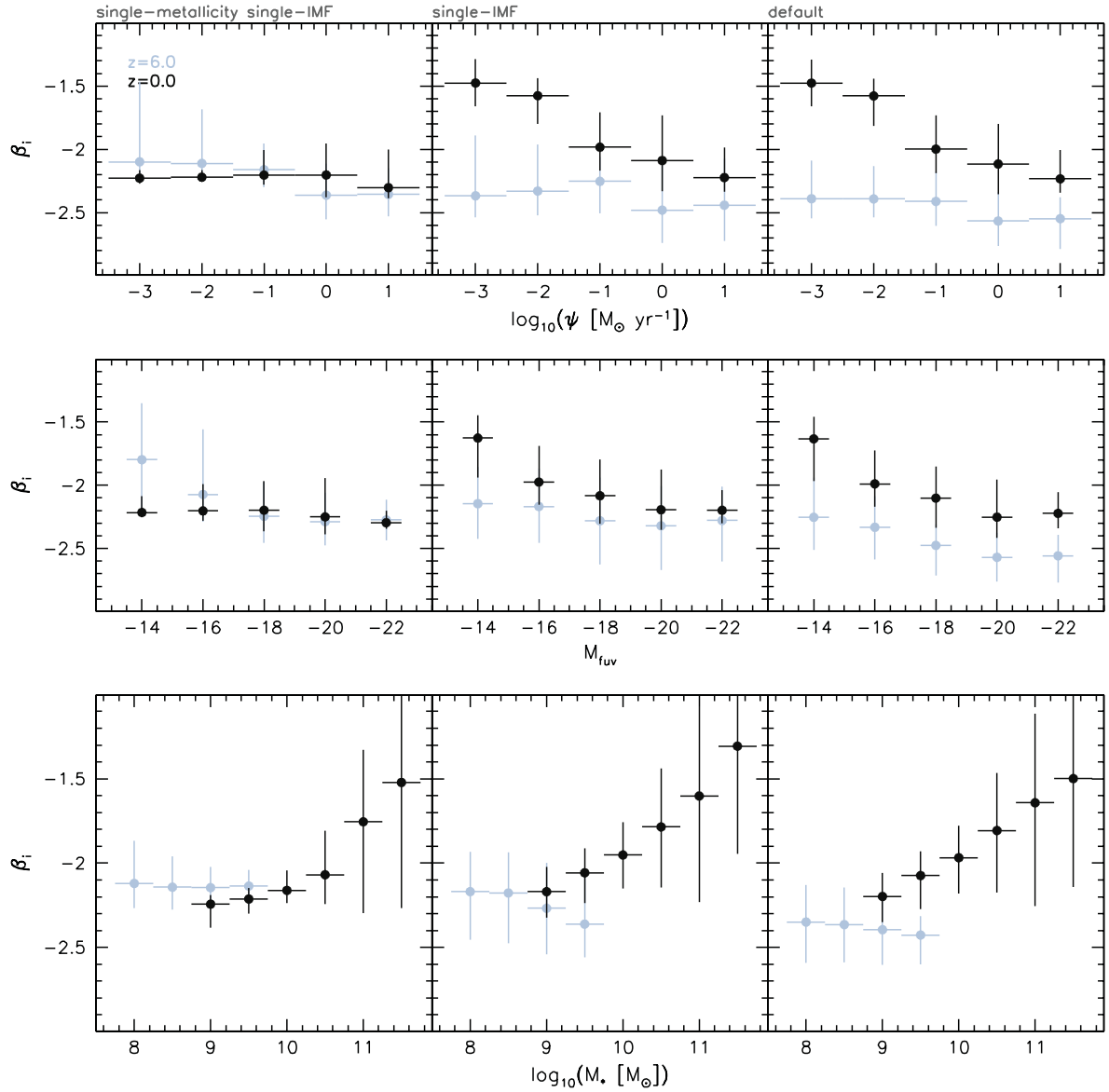

Figure 8. The median intrinsic UVC slope binned by SF rate (top), intrinsic FUV absolute magnitude (middle) and stellar mass (bottom) at $z = 0$ (black) and $z = 6$ (grey) for each of the three model variants: single-metallicity and single-IMF (left), single-IMF (middle) and *default* (right). In each case, the horizontal bar denotes bin width while the vertical bar denotes the 15.87–84.13th percentile range of the GALFORM model predictions.

and *default*) binned by the SF rate, intrinsic UV luminosity and stellar mass, which we discuss in turn below.

4.1 Star formation rate

The top panels of Fig. 8 show the median UVC slope (and the 15.87–84.13th percentile range) for galaxies binned by their SF rate at $z = 0$ and 6 using the three variants of the B05 model (single-metallicity and single-IMF, single-IMF and *default*). For the single-metallicity single-IMF model there is no correlation between the SF rate and median intrinsic UVC slope, irrespective of redshift. However, for both the single-IMF and *default* variants of the model, there is a negative correlation at low redshift. This trend becomes progressively flattened at higher redshift and for $z > 4$ it is essentially flat ($z = 6$ is shown in Fig. 8). The existence of this trend in the single-IMF and *default* variants of the model and its absence in the single-metallicity and single-IMF model suggests this trend is driven by the metallicity variation as a function of the SF rate. At high redshift the variation in metallicity is less pronounced leading to the absence of any correlation.

4.2 Intrinsic UV luminosity

Related to the SF rate but more useful in an observational context is the intrinsic FUV luminosity, $L_{\rm fuv}$. The middle panels of Fig. 8 show the median intrinsic UVC slope binned by the intrinsic absolute FUV magnitude. Due to the close connection between the SFR and the intrinsic UV luminosity, a similar trend exists to that described above; at low redshift there is a mild trend such that more luminous galaxies have an intrinsically bluer UVC colour (in the single-IMF and *default* variants of the model), while at higher redshift the correlation is virtually flat. The flat trend at high redshift reinforces

the conclusions of several studies (e.g. Wilkins et al. 2011b) that galaxies with brighter *observed* UV luminosities have greater dust attenuation than their low-luminosity counterparts.

4.3 Stellar mass

The lower panel in Fig. 8 shows the variation of β with stellar masses for galaxies around M^* at $z = 0$ and 6. At $z = 0$ (but extending to $z \simeq 1$), and for all three model variants, the median UVC colour is also correlated with stellar mass, becoming redder at high-stellar masses. The width (as measured by the confidence interval) of the UVC slope distribution also increases dramatically to high-stellar masses. The fact that this trend exists for all three models suggests that it is driven predominantly by the SFH in so far as more massive galaxies are typically composed of older populations (e.g. Kauffmann et al. 2003). At higher redshift this correlation flattens, to the extent that at $z = 6$, the trend is virtually flat.

One implication of the strong correlation between stellar mass and UVC slope is that assuming a constant intrinsic slope to convert the observed slope to an attenuation may introduce an artificial correlation. As an example, applying the same intrinsic slope found at $\log_{10}(M_*/\mathrm{M}_\odot) = 9$ ($\beta_\mathrm{i} \simeq -2.2$) would result in a systematic overestimation of the attenuation at $\log_{10}(M_*/\mathrm{M}_\odot) = 11$ ($\beta_\mathrm{i} \simeq -1.6$) of $\delta A_\mathrm{fuv} \simeq 1.42$ assuming the single-IMF variant of the B05 model.

4.4 Redshift

Potentially, the most important trend is the evolution of the median UVC slope with redshift. Shown in Fig. 9 is the redshift evolution of the median UVC slope for star-forming galaxies (SFR $> 0.1\,\mathrm{M}_\odot\,\mathrm{yr}^{-1}$) assuming both the single-IMF (solid line) and *default* (dashed line) implementations of the B05 model.

In both cases, the median intrinsic UVC slope evolves, becoming progressively redder towards lower redshift. The cause of this is a combination of both the increasing average metallicity of recently formed stars and the changing stellar mass distribution in star-forming galaxies. As progressive generations of stars form, the mass distribution in galaxies becomes increasingly dominated by low- and intermediate-mass stars with long main-sequence lifetimes. The evolution of the median UVC slope assuming the *default* implementation of the B05 model is similar to the single-IMF implementation of the B05 model, though slightly bluer over the entire history. Specifically, at $z > 1$ the difference between models is significant ($\delta\beta_\mathrm{i} \simeq 0.1$) while at lower redshift ($z < 0.5$) the difference becomes negligible $\delta\beta_\mathrm{i} < 0.05$, reflecting the smaller contribution of merger-driven SF to the total SF rate density at these epochs.

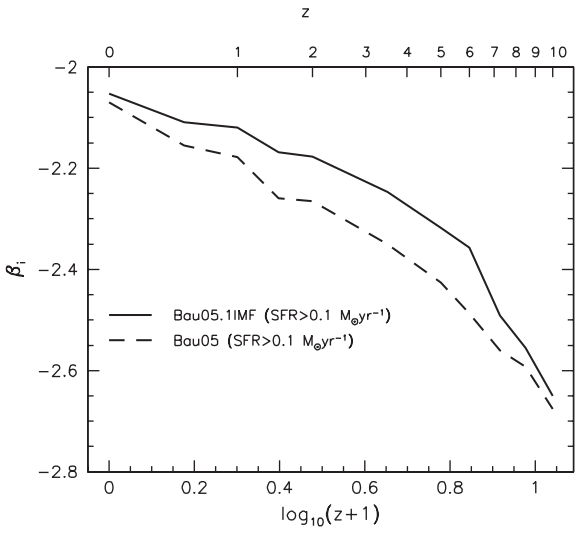

Figure 9. The evolution of the median UVC slope of star-forming galaxies as a function of redshift for both the single-IMF and *default* implementation of the B05 model.

If this decrease in the median-intrinsic UVC slope is not properly taken into account, and, for example, a relation relevant at low redshift is applied to high-redshift galaxies (as is typically done in the literature), the UV attenuation inferred will be systematically underestimated. For example, applying a relation based on the intrinsic UVC slope distribution at $z = 0$ to galaxies at $z = 7$ would result in the systematic underestimation of the UV attenuation by $\delta A_\mathrm{fuv} \simeq 0.97$ and the possible introduction of an erroneous redshift trend or at least an overestimation of the redshift evolution.

In addition, in both cases, the width of the distribution also evolves, becoming slightly narrower at higher redshift (at $z = 6$, $\sigma_\beta = 0.26$, cf. $z = 6$, $\sigma_\beta = 0.30$ for the single-IMF implementation). For the default implementation, we also see the emergence of bimodality in the distribution as a result of the merger-driven SF occurring with a top-heavy IMF. At low redshift, where the contribution of merger-driven SF is small, and at very high redshift, where the contribution of quiescent SF is low, the bimodality essentially disappears.

5 CONCLUSIONS

We have used realistic SF and metal enrichment histories predicted by the GALFORM semi-analytical galaxy formation model to investigate the intrinsic distribution of UVC colours and slopes. We find, for star-forming galaxies at low redshift, that the standard deviation of the distribution of UVC slopes (parametrized by the power-law index β_i) is $\sigma_\beta \simeq 0.30$ (assuming a single IMF). Assuming the C00 reddening curve this suggests an intrinsic uncertainty of $\delta A_{1500} \simeq 0.71$ in the UV attenuation inferred from the UVC slope for an individual object without any additional information to constrain the SF or metal enrichment histories.

We also investigated how the median intrinsic UVC slope and the width of the β_i distribution correlate with various properties including the SF rate, intrinsic UV luminosity, stellar mass and redshift. At low redshift, we find that the median UVC slope is sensitive to the SF rate, intrinsic UV luminosity and stellar mass, with more massive galaxies typically having redder UVC slopes and those with higher SF rates (and higher UV luminosities) typically being bluer. At higher redshift these correlations flatten and become less important. The model also suggests significant evolution of the median UVC slope with redshift (though the width of the distribution changes only mildly). These various correlations suggest that trends of the observed UVC slope with stellar mass or redshift are not driven entirely (if at all) by dust but partly by the evolution of the SF and metal enrichment histories of galaxies. In order to correctly interpret observations, in the context of dust reddening, it is then important to compare the observed distribution of UVC slopes with a model including a physically motivated treatment of dust but taking also into account the predicted intrinsic distribution. In a follow-up paper (Wilkins et al., in preparation), we compare the observed distribution with the predicted intrinsic one for bright $z \approx 3$–5 star-forming galaxies.

ACKNOWLEDGMENTS

We would like to thank the anonymous referee for helpful suggestions and comments which improved the quality of this paper. The calculations for this paper were performed on the ICC Cosmology Machine, which is part of the DiRAC Facility jointly funded by STFC, the Large Facilities Capital Fund of BIS and Durham University. SMW acknowledges support from STFC. VGP acknowledges support from the UK Space Agency. VGP, CGL and CMB acknowledge support from the Durham STFC rolling grant in theoretical astronomy.

REFERENCES

Baldry I. K., Glazebrook K., 2003, ApJ, 593, 258
Baugh C. M., 2006, Rep. Progress Phys., 69, 3101
Baugh C. M. et al., 2005, MNRAS, 356, 1191 (B05)
Benson A. J. et al., 2003, ApJ, 599, 38
Bouwens R. J. et al., 2009, ApJ, 705, 936
Bouwens R. J. et al., 2011, preprint (arXiv:1109.0994)
Bressan A., Granato G. L., Silva L., 1998, A&A, 332, 135
Bruzual G., Charlot S., 2003, MNRAS, 344, 1000
Calzetti D. et al., 2000, ApJ, 533, 682 (C00)
Cardelli J. A., Clayton G. C., Mathis J. S., 1989, ApJ, 345, 245
Cole S., Lacey C. G., Baugh C. M., Frenk C. S., 2000, MNRAS, 319, 168
Dunlop J. S., McLure R. J., Robertson B. E., Ellis R. S., Stark D. P., Cirasuolo M., de Ravel L., 2012, MNRAS, 420, 901
Finkelstein K. D. et al., 2011, ApJ, 742, 108
Finkelstein S. L. et al., 2012, preprint (arXiv:1110.3785)
Fioc M., Rocca-Volmerange B., 1997, A&A, 326, 950
Fioc M., Rocca-Volmerange B., 1999, preprint (astro-ph/9912179)
Hoversten E. A., Glazebrook K., 2008, ApJ, 675, 163
Kauffmann G. et al., 2003, MNRAS, 341, 54
Kennicutt R. C., Jr, 1983, ApJ, 272, 54
Kurucz R. L., 1993, Kurucz CD-ROM, Smithsonian Astrophysical Observatory, Cambridge, MA, c1993
Lacey C. G., Baugh C. M., Frenk C. S., Silva L., Granato G. L., Bressan A., 2008, MNRAS, 385, 1155
Lacey C. G., Baugh C. M., Frenk C. S., Benson A. J., 2011, MNRAS, 412, 1828
Lagos C. D. P., Lacey C. G., Baugh C. M., Bower R. G., Benson A. J., 2011, MNRAS, 416, 1566
Lee J. C. et al., 2009, ApJ, 706, 599
Meurer G. R., Heckman T. M., Calzetti D., 1999, ApJ, 521, 64
Orsi A., Lacey C. G., Baugh C. M., Infante L., 2008, MNRAS, 391, 1589
Parkinson H., Cole S., Helly J., 2008, MNRAS, 383, 557
Salpeter E., 1955, ApJ, 121, 161
Wilkins S. M., Hopkins A. M., Trentham N., Tojeiro R., 2008a, MNRAS, 391, 363
Wilkins S. M., Trentham N., Hopkins A. M., 2008b, MNRAS, 385, 687
Wilkins S. M., Bunker A. J., Ellis R. S., Stark D., Stanway E. R., Chiu K., Lorenzoni S., Jarvis M. J., 2010, MNRAS, 403, 938
Wilkins S. M., Bunker A. J., Lorenzoni S., Caruana J., 2011a, MNRAS, 411, 23
Wilkins S. M., Bunker A. J., Stanway E., Lorenzoni S., Caruana J., 2011b, MNRAS, 417, 717

This paper has been typeset from a TEX/LATEX file prepared by the author.